International Journal of Civil Engineering

Geotechnical Engineering

Numerical modeling of reverse fault rupture propagation through clayey embankments

M. Mortazavi Zanjani[1], **A. Soroush**[2,*]

Received: 2012/08/2, Revised: 2012/08/2, Accepted: 2013/01/14

Abstract

This paper presents results of a thorough study on the phenomenon of rupture propagation of reverse faults from the bedrock foundation through homogeneous clayey embankments, mainly at the end of construction, with complementary analyses for the steady state seepage through the embankment. The study is performed by means of numerical analyses with a nonlinear Finite Element Method, verified beforehand through simulating fault propagations in an existing horizontal soil layer experiment. Multiple cases considering three slopes & three clayey soils for the embankment and five fault dip angles, activated in several locations of base of the embankment, are analyzed. The results show that ruptures in the embankment follow optimal paths to reach the surface and their near-surface directions are predictable with respect to corresponding theories of classical soil mechanics. Various types of rupture in the embankment are produced; on the basis of the rupture types, the embankment base is divided into three distinguishable zones, which can be used for interpretation of fault ruptures behavior. The effects of materials and slope of the embankment, fault dip angle, and fault's point of application in the bedrock-soil interface on the rupture paths are studied in depth.

Keywords: *Fault rupture propagation, Numerical modeling, Embankment.*

1. Introduction

In the course of an earthquake, strong ground shaking is the principal source of damage over a widespread area, affecting different structures. Meanwhile, a zone around the fault line is exorably involved in local hazardous permanent offset of the fault. Naturally, the main focus of earthquake engineering has been the former, while mitigation of fault rupture damage was regarded to be far from earthquake engineering practice. However, the effect of fault rupture, especially on important structures such as pipelines, bridges and dams, is more severely felt during the last two decades [1-3]. The existence of faults in dam foundations is particularly prevalent in earthquake-prone areas. "Of the hundreds of dams built in regions of high earthquake potential, there are few in locations where faults were not recognized or suspected to exist[4]. According to Louderback [5], in the Coast Ranges of Central California, the most preferable alternatives for dam sites from topographical point of view are located in fault line valleys. Furthermore, some unmapped branches ofactive faults may be disclosed only during detailed geological surveys or in the course of excavating dam's foundation, rendering the allocated time, energy and money worthless [6,7]. In addition, blind fault lines [8] and new extensions of existing faults during new earthquakes [9] should be taken into account.

Although not catastrophic, there have been dams experiencing fault rupture dislocation under their foundations [3,6]. Moreover, numerous new dams are under construction or design, in seismically active regions in the vicinity of faults. As an example,the 148 m high Rudbar Lorestan Dam, and its power plant within the Zagros fold and thrust belt in the central part of Iran can be mentioned [10].

Hitherto, fault rupture propagation through a uniform horizontal soil layer has received plenty of attention in antecedent researches. Pertinent field investigations have focused mainly on evidences from surface and trench observations [6,11] whereas physical models [6,8,12-15] and numerical studies[2,8,14-20] have attempted to examine the direction and pattern of fault propagation in the top soil layer.

Louderback [5] first observed effects of active fault displacement in the underlying bedrock on earth dams. This topic was further pursued by [3,4,21-23].

* *Corresponding Author: soroush@aut.ac.ir*
Department of Civil and Environmental Engineering, Amirkabir Universityof Technology, Tehran, Iran

Chenney et al.[24]studied strike-slip fault rupture via centrifuge tests on loamy (silt-clay) embankment models. Their preliminary observations suggested damage patterns for rupture propagation in simple homogenous embankments.

Sohn [25] continued their work by adding a reservoir to study strike-slip fault rupture propagation during steady state seepage conditions, accompanied by 3D FEM (Finite Element Method) numerical simulations.

Lazarte [8] performed field, numerical and experimental studied on strike-slip fault rupture through embankments to overcome the inherent limitations in any one method. He carried out a 1-g physical modeltest on a saturated clay embankment in order to establish correlations between the displacement imposed along the base rock and the resulting breakage pattern on the structure surface. The 2D and 3D numerical modeling facilitated the assessment of the effects of material properties, geometry and kinematic conditions.

A case study of the Aviemore Dam in New Zealand regarding the effect of foundation fault rupture on the dam, as well as stability of the dam under strong ground motions was given by Mejia et al.[26].

Zania et al [27]carried out a simple numerical study on 45° and 60° normal and reverse fault rupture propagation in a 3H:1V dense sandy embankment for two positions of fault in the embankment baseand presented vertical displacements of the surface.

Physical and numerical studies of strike-slip fault rupture propagation through embankment dams have received much attention; nonetheless, the findings have limited applications for dip-slip faults owing to fundamental differences between the slip mechanisms. Although case studies, e.g. Aviemore Dam, help provide a real insight into the dams behavior during faulting, they fall short of delicately explaining rupture propagation in embankments. The limited existing numerical analyses on dip-slip faults, e.g. [27], do not include investigations on the effect of different geometrical and mechanical aspects of the problem.

A systematic study of dip-slip fault rupture propagation through zoned earth dams is better achieved through taking simplified steps; i.e., modeling a plane strain geometry of a homogeneous compacted clayey embankment. This keeps computational efforts at a reasonable limit, facilitating the study of effects of different fault and soil parameters (such as fault dip angle, fault location and soil characteristics), and eliminates minor and local features of faulting.

The most similar practical case to this desired simplicity is an embankment dam at the end of construction. During construction, embankment layers are compacted in a near optimum moisture content (usually w_{opt} +2%), with saturation degrees ranging approximately between 85 and 92%. Excess pore water pressure build-up within the embankment is monitored during construction to control the construction speed. The soil is nearly saturated, especially at the embankment base where the highest localized strains develop during faulting. Therefore, fault activation immediately at the end of construction occurs in un consolidated undrained conditions, UU, where internal friction angleis almost negligible. The constant cohesion and zero friction angle are thus selected for this condition.

To cover more practical aspects of embankment dam engineering, complementary analyses of fault activation during steady state seepage condition is also introduced. Here, coupled pore pressure-stress analyses are performed and the effective soil parameters are adopted.

In this paper, fault rupture propagation through a homogeneous clayey embankment is analyzed numerically using the Finite Element Method. The present study do not account for effects of strong ground motion in the vicinity of fault as discussed in [28]; i.e. it mainly focuses on the quasistatic dislocation of fault under the embankment and its potential risk to the soil structure. In order to gain a comprehensive perspective, embankments with three different clayey materials and three values of surface slopes, subjected to differently oriented reverse faults activated at different locations of the embankment base, are studied. The embankment is supposed to overly horizontal bedrock so the effects of bedrock inclination ,[29], is not included. Results of the analyses are presented in forms of contours of maximum strain and their core lines as representatives of rupture paths. The above immediate results of our analyses are studied in depth from two points of view: “near surface slope of rupture” and “path and shape of rupture within the structure”. Discussions and conclusions on the results are finally presented.

2. Problem description and geometry

A 10m high clayey embankment is assumed to overly bedrock having a potentially active fault.The fault movement, reaches the bedrock-soil interface on the left side of the dam, while the right side of the model is fixed. Plane strain conditions govern the embankment geometry. Fig. 1 presents a typical geometry, boundary conditions and FE idealization of the model.

An active fault may exist in any place along the embankment base. The location of the fault displacement is determined by D, measured from three different datums. Therefore, fault displacement is applied at different base points, the position of which is introduced by three separate axes; two axes staring at the toe and heel symmetrically for the upstream and downstream slopes and the other axis for the crest area. Five dip angles are assumed as α =30°, 45°, 60°, 75°, 90° .

The model is simulated with three different surface slopes: 2H:1V,2.5H:1V and 3H:1V. The domain is discretized with bilinear quadrilateral elements with an average size of 0.25m generating 4111, 5263, 6082 elements for the 2:1, 2.5:1 and 3:1 slope embankments, respectively.

2.1.Soil characteristics and constitutive model

The Finite Element Code Abaqus [30] and the Mohr-Coulomb elastic-perfectly plastic constitutive model with a non-associated flow rule have been incorporated in this study. The Mohr-Coulomb yield surface is implemented wherein the flow potential function is hyperbolic and smooth elliptical in the meridional and deviatoric stress planes,

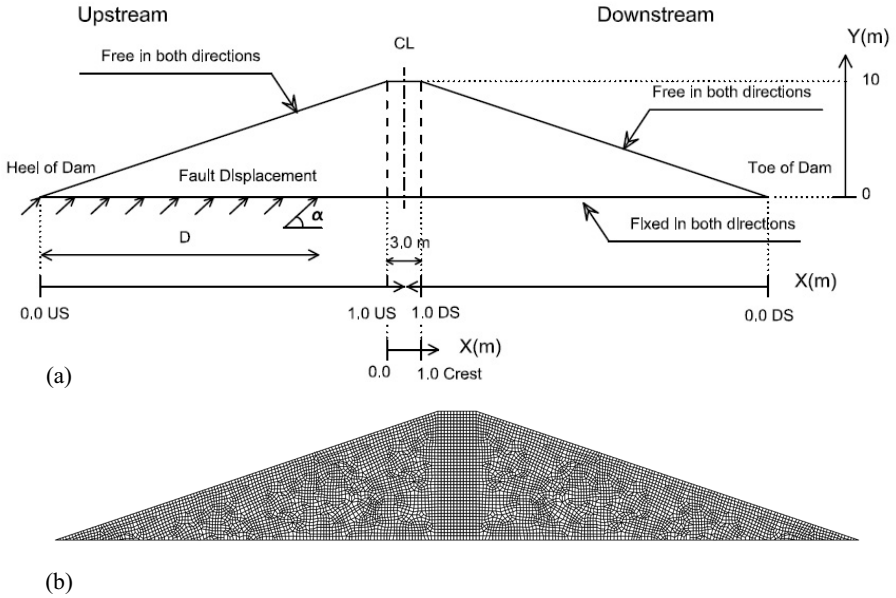

Fig. 1 (a) Embankment model and boundary conditions with three separate horizontal axes as references for fault application points, D, in upstream (US), crest and downstream (DS) and (b) meshing of the model in slope 3:1

respectively [31]. Thus:

$$G = \sqrt{(\epsilon c|_0 \tan\psi)^2 + (R_{mw} q)^2} - p\tan\psi \quad (1)$$

Where,

$$R_{mw}(\Theta, e) = \frac{4(1-e^2)\cos^2\Theta + (2e-1)^2}{2(1-e^2)\cos\Theta + (2e-1)\sqrt{4(1-e^2)\cos^2\Theta + 5e^2 - 4e}} R_{mc}(\frac{\pi}{3}, \phi) \quad (2)$$

$$R_{mc}(\frac{\pi}{3}, \phi) = \frac{3-\sin\phi}{6\cos\phi} \quad (3)$$

and, Θ is the deviatoric polar angle defined as:

$$\cos(3\Theta) = \left(\frac{r}{q}\right)^3 \quad (4)$$

Where, *p, q, r* are the first, second and third invariants of stress, respectively; is the angle of friction; φ is the angle of friction; ; *c* is cohesion of soil; ψ is cohesion of soil; $c|_0$ is the initial cohesion yield stress, i.e. $c|_0 = c|_{\bar{\varepsilon}^{pl}=0}$, where $\bar{\varepsilon}^{pl}$ is equivalent plastic strain, and ϵ is the meridional eccentricity that defines the rate at which the hyperbolic function approaches the asymptote. *e* is a parameter, referred to as the deviatoric eccentricity, that describes "out-of-roundedness" of deviatoric section in terms of the ratio between shear stress along the extension meridian (Θ=0) and shear stress along the compression meridian (Θ=π/3). Other mechanical parameters of the three types of clayey materials are introduced in Table 1.

2.2. Loading and fault displacement

First the initial state of stress in the embankment was set up by the switch on gravity technique. Thereafter, the base displacement induced by faulting was applied incrementally to the left side of the model (i.e., hanging wall), as shown in Fig. 1-a. The amount of base displacement required for rupture propagation through the structure has been a matter of question among researchers. For uniform horizontal layers of cohesionless materials,a vertical displacement of 2 to 6% of height of the overlying layer has been agreed as a proper value [6,12,20]. According to Bray et al. [6] comparatively higher base displacements, i.e. 10-16% of the height, are needed for horizontal layers of saturated clayey materials. However, materials commonly used in embankments are stiffer than saturated clayey materials in experiments. Preliminary analyses of this study revealed that smaller base displacements are sufficient for development of rupture through the trapezoidal geometry of embankments of this study. Therefore, predicated on sensitivity analyses, a vertical displacement equivalent to 4% of the structure's height was selected throughout the analyses.

2.3. Mesh dependency

Effects of mesh size on fault rupture propagation in the embankments have been studied through varying mesh

Table 1 Soil parameters used in unconsolidated undrainednumerical analyses ofembankments

Material	Abbreviation	$\gamma(kN/m^3)$	$c(kPa)$	$\varphi(°)$	$\psi(°)$	$E(MPa)$	ν	K_0
Medium Stiff Clay	MSC	19	40	0	0	10	0.49	0.7
Stiff Clay	SC	20	80	0	0	20	0.45	0.7
Very Stiff Clay	VSC	21	120	0	0	30	0.4	0.7

densities. Sensitivity analyses were carried out for the different embankment surface slopes, material type sand fault dip angles. Fig. 2 shows typical results for α=30° activated at D=0.8 US in the medium stiff clay embankment with 3:1 slope. The results are compared in the form of maximum strain for three different average mesh sizes, 15, 25 and 50 cm. The shear zone of 50 cm mesh size is much diffused while 25 cm mesh gives a comparatively narrower shear band. The shear band description of 15 cm mesh is slightly more concentrated than that of 25 cm, yet with a threefold number of elements and higher computational costs.Thus, the mesh size of 25 cm was deemed both sufficiently accurate and computationally efficient for further analyses.

3. Verification

The modeling scheme and analysis technique were verified by numerical simulation of the Bray et al. experiments [6]. The clay-box model test apparatus of Bray et al. was 107 cm long, 61 cm high, and 30.5 cm wide and housed a weak, saturated clay layer that exhibited suitable and controllable stress-strain behavior. Values of mechanical soil parameters were reported as, γ=15.7 kN/m^3, c=1.63kPa, φ=ψ=0°, v=0.49 and K_0=0.89.

Fig. 3 compares results of our study and the experiments, in the context of maximum strain contours. Simply due to the complex nature of soils, a slight difference is observed between the rupture paths in front side and back side of the clay box test; the latter is selected for comparison.The comparisons are made from three points of view: rupture paths, surface outcrops and tension cracks. Rupture paths and surface outcrops resulted from ouranalyses are in good agreement with those of the experiments. Multiple tension cracks are formed in 90° fault on top of the clay box in the hanging wall side that coincide with the zone of high strains in the left hand side, resulted from the numerical analysis.

4. Results

Different researchers have used various numerical results to pursue fault rupture paths, for instance; Bray et al. [6], Lazarte [8], Lin et al. [14], and Loukidis et al. [20] employed contours of shear stress and maximum shear strain, maximum shear stress, plastic strains, and maximum shear strains, respectively.

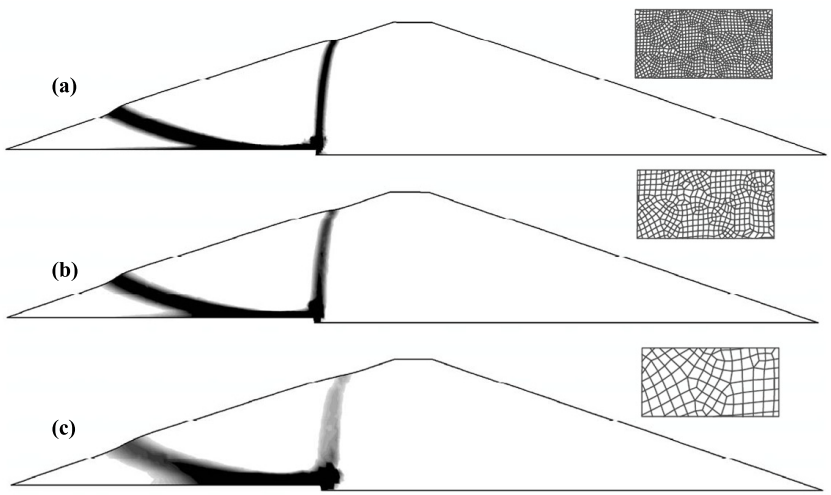

Fig. 2 Sensitivity analysis on the effect of mesh density (contours of maximum strain ranging from 0.05 to 0.15 for 30° fault activated at D=0.8 US in medium stiff clay embankment with 3:1 slope at 4 percent vertical base displacement) with mesh size (a) 0.15m, (b) 0.25m, (c) 0.5m

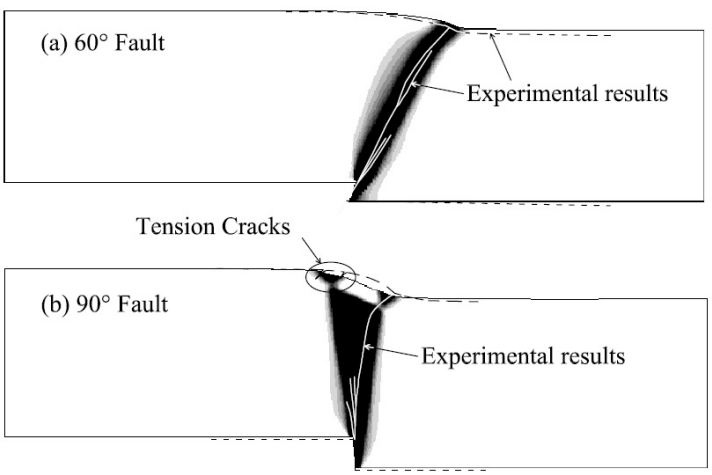

Fig. 3 Numerical results of fault rupture through saturated clay in comparison with experimental result of Bray et al. (a) 60° fault (b) 90° fault

In general, stress interpretations of rupture are diffused and cannot locate a localized zone whereas strain interpretations depict localized paths [6,20]. This was similarly noticed in our simulations. Furthermore, among strain descriptions of fault rupture, maximum shear strains and maximum shear strain rates offer the most realistic representation of fault rupture paths[20]. Herein, the former one is selected.

Figs. 4 to 6, typical results of the analyses, present rupture propagation paths in the form of contours of maximum stains within the embankment of medium stiff clay with 2.5:1 surface slopes, when respectively 30°, 60°, 75°reverse faults are activated at different locations of the embankment base. The general shape of similar results for α=45° and 90° for this embankment and for all five values of αfor the other embankment cases (with 2:1 and 3:1 surface slopes; and stiff and very stiff materials) are the same.

The above immediate results of our analyses may be studied in depth from two points of view: "near surface slope of rupture"and"path and shape of rupture within the structure". These two concepts will be elaborated in the following sections. Hereafter, the rupture path is meant by the line passing through center of maximum strain contour with the highest value (the most inner contour).

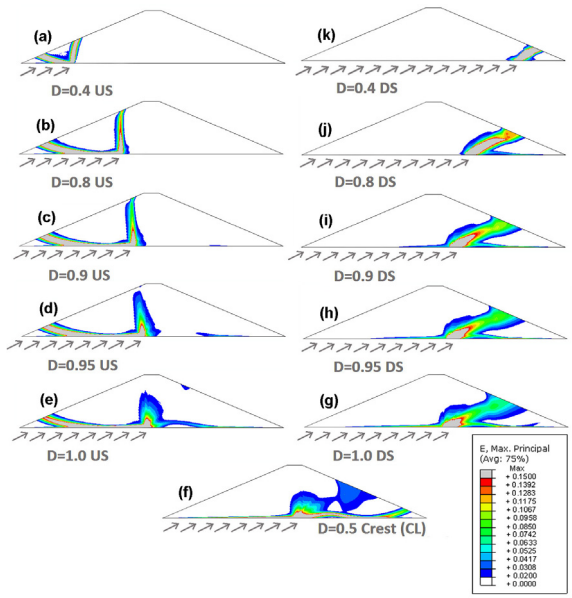

Fig. 4 Rupture propagation of 30° reverse fault in medium stiff clay dam with slope 2.5:1; 'D' represents the location of fault in base, introduced in Fig 1

4.1. Near surface slope of rupture

Figs 4 to 6 suggest that rupture paths rotate while approaching the embankment surface. This has been previously captured by Cole and Lade [12]in their experiments on horizontal sandy soil layers.

Failure surfaces resulted from the activation of reverse faults correspond to the passive state in soils. According to Rankine's Theory, when a soil mass is forced to fail in the passive state, as shown in Fig. 7-a for a horizontal soil layer, failure surfaces are formed in a direction making an angle of λ=45°-φ/2 with direction of the maximum principal stress. Contemporary researches [12,32,33] suggested that λ is more realistically represented as λ=45°-ψ/2, where ψ is the soil dilation angle.

When the soil surface is sloping, principal stresses are parallel and normal to the surface (Fig. 7-b); therefore the rupture angles are λ=45°-ψ/2± β with respect to the horizontal line, where β is the soil surface slope.Considering that for clayey materials ψ=0°, values of λ=45°± β are calculated and summarized as λ_1 and λ_2 in Table 2 for the embankments with the three slope values.

The results of present numerical analyses indicate that near the surface, sufficiently far from the imposed boundary conditions of fault displacement, rupture paths follow the

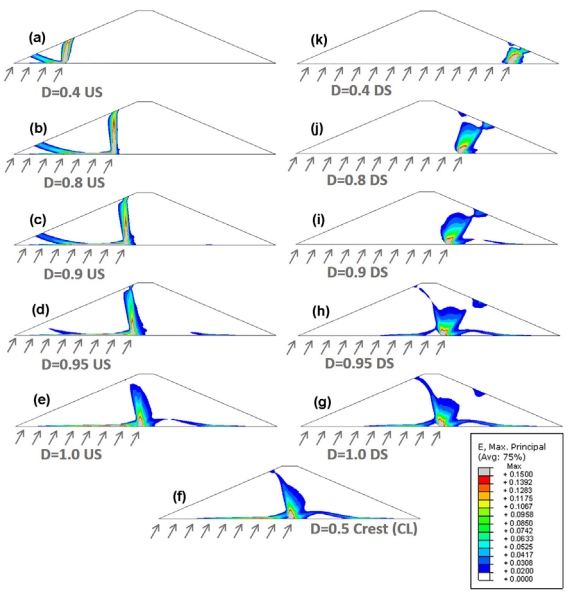

Fig. 5 Rupture propagation of 60° reverse fault in medium stiff clay embankment with slope 2.5:1;'D' represents the location of fault in base, introduced in Fig 1

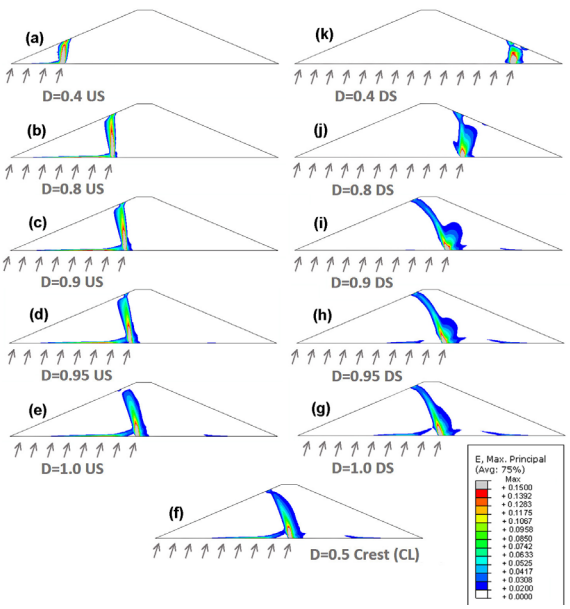

Fig. 6 Rupture propagation of 75° reverse fault in medium stiff clay embankment with slope 2.5:1;'D' represents the location of fault in base, introduced in Fig 1

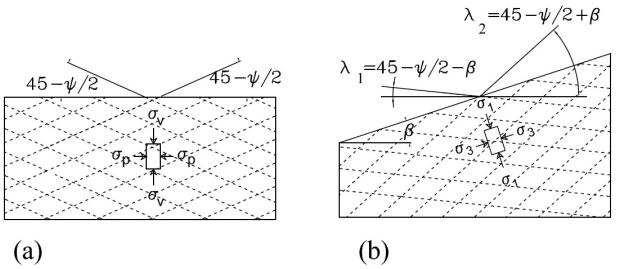

Fig. 7 Failure surfaces for passive state (a) in horizontal soil layer (b) in sloping surface

above failure directions. This was shown by Mortazavi et al. [34] for horizontal sand deposits.

Fig. 8 compares theoretical failure directions with general rupture propagation paths (with reference to Figure 5)for the embankment of medium stiff clay with 2.5:1 slopes when a 60° reverse fault is activated at different locations of the embankment base. As it is evident, surficial parts of the rupture paths are running parallel to the theoretical failure lines. To make it quantitative, near-surface slopes of ruptures are measured for the five fault dip angles activated at seven different locations of the embankment base and compared with their corresponding theoretical λ_1 and λ_2 values in Fig. 9; where solid lines correspond to angles λ_1 and λ_2 for each slope and dashed lines correspond to angles λ_1 and λ_2 for the other two slopes (2:1 and 3:1). The concentration of points corresponding to λ values resulted from our analysis around λ_1 and λ_2 solid lines are obvious for each embankment slope.

4.2. Rupture paths in embankment

The rupture paths in Figs. 5-a to 5-d develop in two branches, a subvertical branch and a subhorizontal branch, both toward the upstream.The subvertical branch rotates near the slope surface, creating a convex curvature looking from the heel and the subhorizontal branch has a concave upward curvature which cuts the slope surface at the embankment heel.When fault location approaches the embankment central line, Figs. 5-e and 5-f, a mild change in the propagating curvature from convex to concave is observed as the subhorizontal branch almost disappears. As the fault line moves downstream,Fig. 5-g,a nascent branch develops toward the downstream slope and it intensifies while the upstream branch fades gradually, Fig 5-h.Further, the upstream branch disappears and rupture develops, with one or two branches, completely towards the downstream slope, as shown in Figs. 5-i to 5-k.

The same discussion applies to the rupture propagation for the 30° reverse fault and the same embankment, except that the rupture path turns towards downstream comparatively earlier, as shown in Fig. 4, 4-f. Moreover, when the fault locates in the downstream zone, only one branch forms towards the slope (Figs. 4-g to 4-k).

For the 75° reverse fault (Fig. 6),more or less similar paths are resulted. For this case, however, subhorizontal branches almost do not form. Moreover, rupture paths turn towards the downstream slope only when the fault is located far in the downstream base (Figs. 6-j and 6-k).

Considering Figs. 4 to 6, one may classify the above rupture propagation paths into three distinguished types:

• Upstreamtype: the upstream type can be seen in Figs. 4(a to d), 5(a to d), and 6(a to d), developing with one or two branches towards the upstream slope. The subhorizontal branch fades as the dip angle increases.

• Intermediate type: fault activation in the middle part of the embankment affects central region as well as upstream and downstream slopes. Mostly, two branches of rupture develop

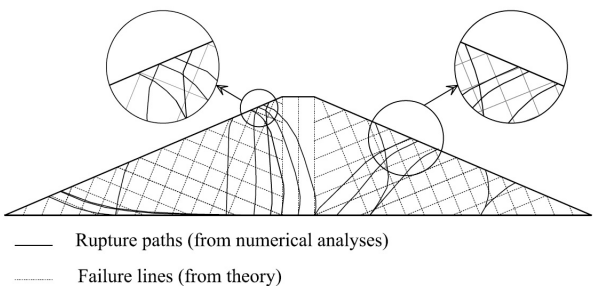

Fig. 8 Comparison between the near surface rupture paths and failure lines, for application of 60° reverse fault at different locations of base of the medium stiff clay embankment with slope 2.5:1

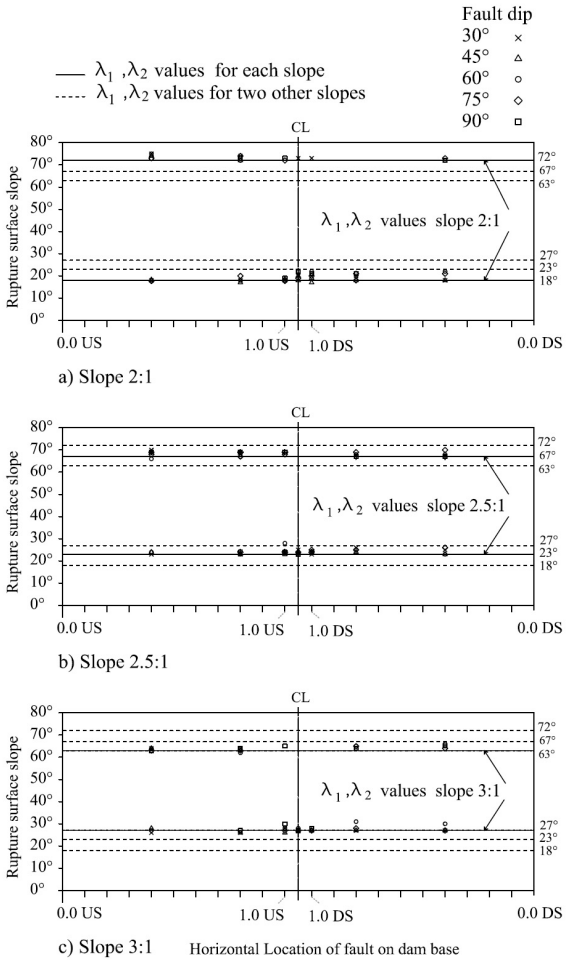

Fig. 9 Near Surface slope of rupture: Comparison of numerical results with λ_1 and λ_2 values for different fault dip angles for the medium stiff clay embankments with slopes of a) 2:1 b) 2.5:1 c) 3:1

that entangle both upstream and downstream slopes (e.g., Figs. 5-g and 5-h). However, in some cases, the downstream branch does not form,whereas the upstream branch is concave,looking from the embankment heel (Figs. 5-f and 6-f).

• Downstream type: the rupture with single or double branches develops completely toward the downstream, as shown in Figs. 4-g to 4-k, 5-i to 5-k and 6-j to 6-k.

The foregoing rupture paths classification suggests one to split base of the embankment into three zones; namely upstream, intermediate and downstream zones. This has been plotted in Figure 10 as the diagram of "fault dip angle" versus "location of fault on the embankment base", for the embankments with the medium stiff clayey material.

Fig. 10 suggests that (1) the Intermediate Rupture Zone (IRZ) becomes narrower as the embankment slope increases; (2) IRZ is wider for the higher dip angles and (3) as the fault angle increases, IRZ tends to downstream of the embankment. The only exception is the anomaly for the embankment with 3:1 slope and dip angle of 45°.

Fig. 11 compares the above zones for the embankments with 2.5:1 and the three types of clayey materials. As the material becomes stiffer, the IRZ becomes narrower and its boundaries move toward the upstream. This different behavior may be attributed to the fact that the stiffer materials behave more brittle during rupturing and therefore the rupture paths leans more to follow straight lines.

4.2.1. Effects of fault dip angle on rupture path and surface displacement gradient

Figs 12 to 14 present typical rupture paths (for the five values of fault dip angle) and their corresponding surface displacement gradients within the embankment of medium stiff clay with 2.5:1 slope, when the fault is activated in the upstream (D=0.8US), middle part (D=0.5Crest), and downstream (D=0.8DS), respectively.

The fault paths in the upstream zone are almost independent of fault dip angle (Fig. 12-a). As it was mentioned in Section 4.2, the subhorizontal branch does not form for large dip angles, 70° and 90°.

In the intermediate rupture zone (Fig. 13-a), the branch turning toward the upstream is nearly independent of fault dip angle. The other branch, developing toward the downstream, tends to follow more or less the fault activation dip angle and rotate as it approaches the slope surface, resulting in different rupture paths.

In the downstream rupture zone (Fig. 14-a), rupture paths start approximately with the fault dip angle and they reach the surface along the predefined failure surfaces (see Section 4.1). In this zone the rupture paths are highly influenced by the fault dip angle. While for the relatively small and relatively large dip angles only one rupture path develops, for the intermediate values of two branches are induced.

With regards to surface displacement gradients, Figs 12-b, 13-b and 14-b are complementary results and indicate maximum gradients of surface displacements and their locations on the embankment surface for the five values of fault dip angles. It can be observed that the fault angle and its activation location at the embankment base have influenced the results.

5. Discussions on fault rupture propagation

Although fault rupture paths in horizontal soil layers may deviate slightly from the straight fault plane projection in the bedrock, the overall fault direction is followed. On the contrary, rupture paths in embankments experience significant deviation from the fault direction and even turn to the opposite side, due to the sloping surface boundary conditions of the structure.For instance, in Fig. 4-a, the rupture path develops through two branches none of which is in the direction of fault

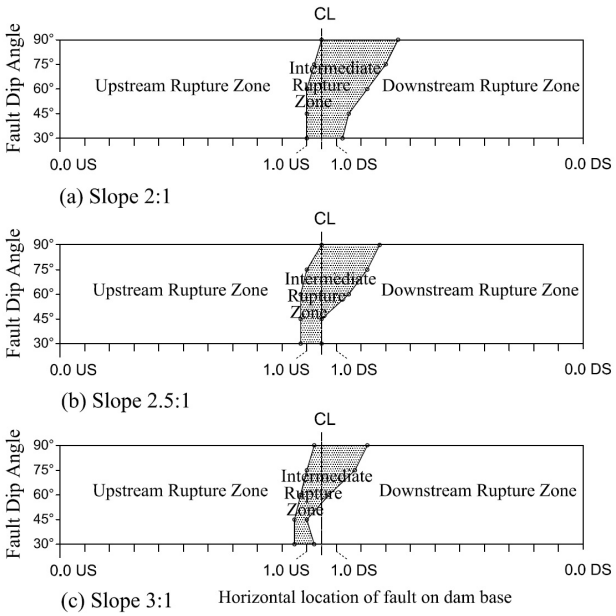

Fig. 10 Zoning of the medium stiff clay embankment to upstream, intermediate and downstream rupture zones for 5 different fault dip angles in different embankment slopes (the intermediate part is coloured gray for better recognition)

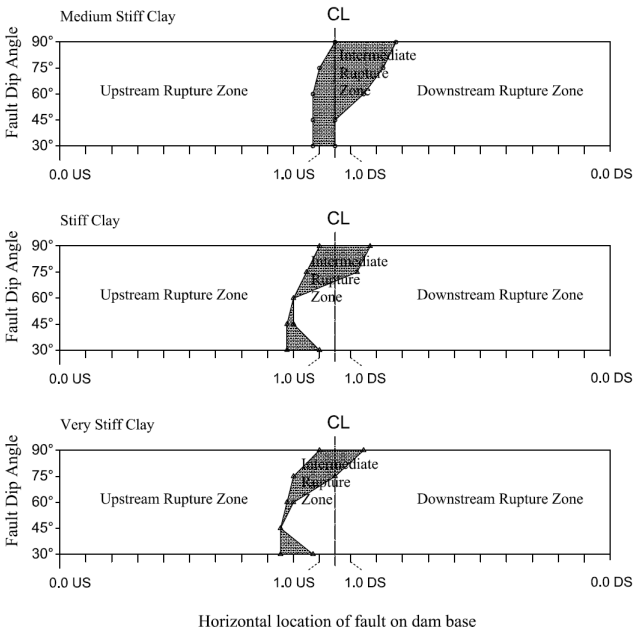

Fig. 11 Zoning of base of 2.5:1 embankments to three zones in 5 different fault dip angles in different soil materials (the intermediate part is coloured gray for better recognition)

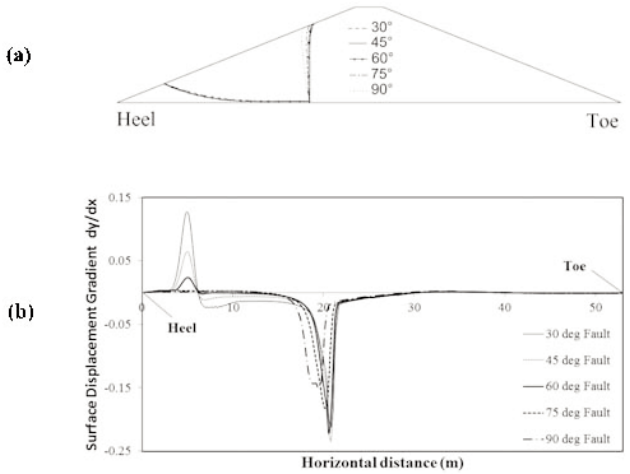

Fig. 12 Effect of fault activation (Upstream Rupture Zone, D=0.8 US) on the medium stiff clay embankment with 2.5:1 slopes (a) schematics of rupture paths (b) surface displacement gradient

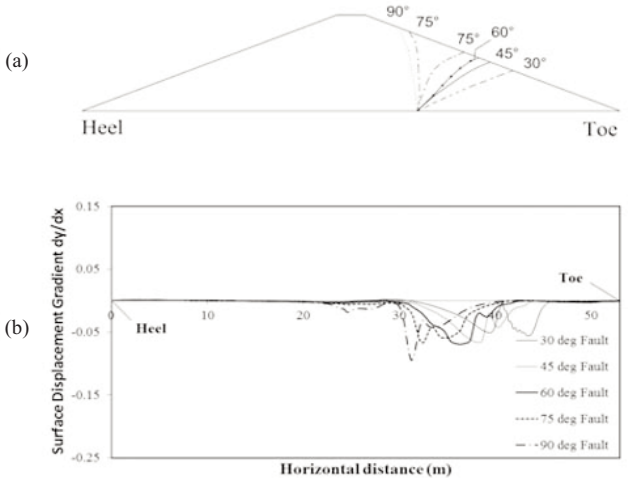

Fig. 14 Effect of fault activation (Downstream Rupture Zone, D=0.8 DS) on the medium stiff clay embankment with 2.5:1 slopes (a) schematics of rupture paths (b) surface displacement gradient

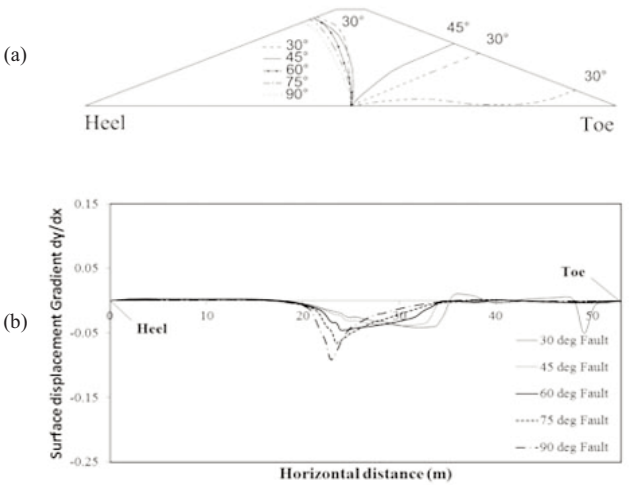

Fig. 13 Effect of fault activation (Intermediate Rupture Zone, D=0.5 Crest) on the medium stiff clay embankment with 2.5:1 slopes (a) schematics of rupture paths (b) surface displacement gradient

plane. Another example isFig. 6-f in which rupture path turns to the opposite side towards the upstream slope.

Fig.15-a sketches potential fault rupture propagation paths within the upstream zone of the embankment. If path I (the fault direction) is to be followed, the rupture should traverse a long path, with a comparatively high average confining stress along the path. Moreover, the volume of soil involved in the rupture process along this path (dashed area) is comparatively large. The combined effects of these two factors make path II, with smaller volume of soil involved (dotted area),preferable for the fault rupture propagation. However, this path is steeper than the fault dip and can only interpret vertical component of the displacement; therefore, a secondary subhorizontal path forms (path III), particularly for smaller dip angles.

In the intermediate zone, as depicted in Fig.15-b,rupture tends to follow a path similar to path IV (in less stiff materials) and path II (in stiffer materials) though path I is in the direction of fault. From a theoretical perspective, rupture path may not follow path I, since its near surface slope is not compatible with λ_1 and λ_2 angles. Two alternative paths are II and III which are more compatible with steeper faults and less steep faults, respectively.

A comparison between paths II and IV reveals that the length of the two paths are almost equal, but the volume of soil involved in path IV (dotted area) is less than that of path II (dashed area); therefore, path IV is followed for a sufficiently flexible material,in which sharp turns are more feasible. In very stiff clay, which behaves more brittle, rupture path does not turn easily towards the opposite direction to follow path IV; thus path II is inevitably formed.

A Similar interpretation, as suggested for the upstream and intermediate zones, applies for the downstream zone; this is

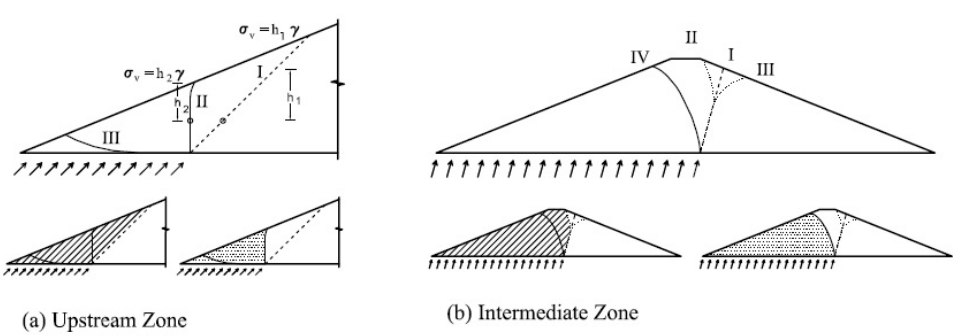

Fig. 15 Possible paths of fault rupture propagation in different parts of the embankment

not given here for the purpose of brevity.

6. Steady State seepage analysis

For the analysis of fault activation during steady state seepage conditions, the coupled pore fluid-effective stress analysis is performed. In this regard effective soil parameters are introduced to the code.

Results of the analysis for the medium stiff clay (2.5:1 slope)and five fault dip angles activated at the centerline of the dam are presented in Fig 16 where effective soil parameters are, φ'=28°, c'=6*kPa*, E'=6*MPa* and ν'=0.3. Areas of small strains are seen around the main localized zone in Fig. 16. This was seen more or less in other cases of fault rupture propagation in the steady state seepage condition and could be attributed to the effect of pore water pressure changes due to faulting.

Figs. 16-a, 16-c and 16-d may be compared to Figs. 4-f, 5-f and 6-f respectively. It is seen that rupture path turns completely toward downstream in Fig. 4-f and toward upstream in Figs. 5-f and 6-f, while in Fig 16 both subvertical and subhorizontal branches exist, with different participation percentages for different fault dip angles; i.e. stronger subhorizontal branch for smaller dip angles and stronger subvertical branch for higher dip angles.

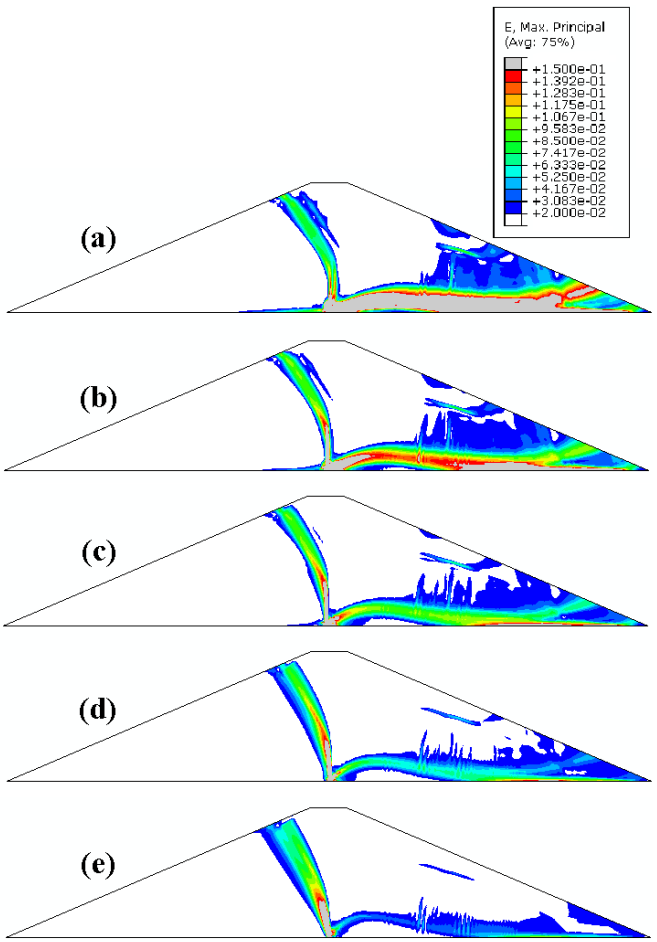

Fig 16. Rupture propagation of reverse fault in steady state seepage for medium stiff clay dam with slope 2.5:1 activated at the centerline of the dam (a) α=30° (b) α=45° (c) α=60° (d) α=75° (e) α=90°

Fig. 17 shows surface displacement gradients when the fault is activated in D=0.8US, D=0.5Crest and D=0.8DS, respectively. Fig 17-a to 17-c show more or less similar trends for the five dip angles, indicating that the dip angle does not have significant effects on the rupture path and its outcrop.

7. Conclusion

Numerical simulation of reverse fault rupture activated in different locations of base of homogeneous embankments for three slopes of embankment, three clayey materials and five dip angles were carried out in this study. The main focus of this study is the dam condition at the end of construction while complementary analyses for the steady state seepage condition are also introduced. The numerical method was verified successfully by predicting fault rupture propagation through existing uniform soil layer experiments. Fault rupture in embankments was studied through two aspects:

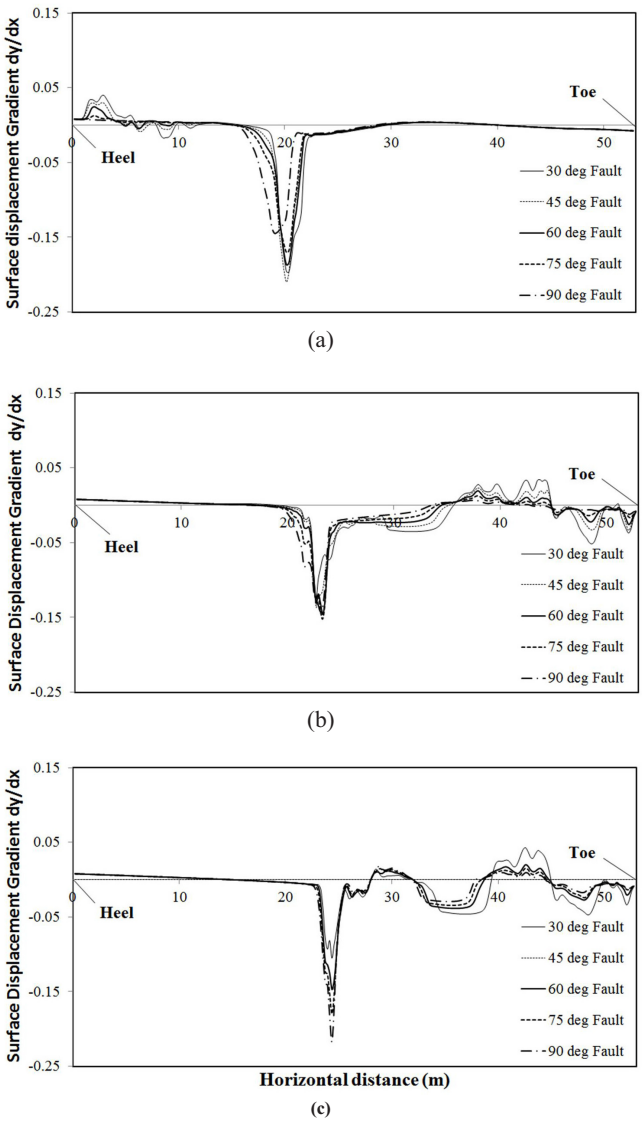

Fig 17. Surface displacement gradient of fault activation in steady state seepage for the medium stiff clay embankment with 2.5:1 slopes (a) D=0.8US (b) D=0.5Crest (c) D=0.8DS

"near surface slope of rupture" and "path and shape of rupture within the structure".

The results showed that the slope of rupture path near the embankment surface is independent of the location and dip angle of fault and rather follows a path which depends on the embankment slope and materials. This fact was justified with theoretical aspects of soil mechanics.

Through the study of various rupture paths and formation of different rupture branches in trapezoidal geometry of the embankment, three different types of rupture propagation and consequently three different zones within the embankment were recognized. The boundaries of the zones were shown to be sensitive to parameters, such as fault angle, embankment slope and material.

The effects of fault dip angle on rupture path within the above three rupture zones are different. For the condition at the end of construction, in the upstream rupture zone the rupture path is independent of fault dip angle. In the intermediate rupture zone, the branch developing toward upstream slope is nearly independent of fault dip angle whereas the downstream branch of rupture is influenced by the fault dip angle. In the downstream rupture zone the rupture path depends on the fault dip angle. During steady state seepage condition rupture paths are independent of fault dip angle while participation percentages of each branch depend on fault dip angle

Acknowledgment: The authors would like to thank Mrs. Roya Solhmirzai for her assistance in technical part. The help of Dr. Anooshiravan Ansari and Dr. Piltan Tabatabaee Shoorijeh for reviewing the manuscript is also gratefully acknowledged.

References

[1] Bray J.D., Seed R.B., Cluff L.S., Seed H.B., Earthquake Fault Rupture Propagation Through Soil, Journal of Geotechnical Engineering, 1994;120 (3), 543-561.

[2] Anastasopoulos I., Gazetas G., Bransby M.F., Davies M.C.R., El Nahas A., Fault Rupture Propagation Through Sand: Finite-Element Analysis and Validation Through Centrifuge Experiments, Journal of Geotechnical and Geoenvironmental Engineering, 2007; 133 (8), 943-958.

[3] Wieland M., Brenner R.P., Bozovic A., Potentially Active Faults in the Foundation of Large Dams Part I: Vulnerability of Dams to Seismic Movements in Dam Foundation. Proceedings of the 14th International Conference on Earthquake Engineering, 2008; Beijing, China.

[4] Sherard J.L., Cluff L.S., Allen C.R.,Potentially Active Faults in Dam Foundations, Geotechnique, 1974; 24, 367-427.

[5] Louderback G.D., Characteristics of Active Faults in the Central Coast Ranges of California, with Application to the Safety of Dams. Bulletin of the Seismological Society of America, 1937;27 (1), 1-27.

[6] Bray J.D., Seed R.B., Seed H.B., The Effect of Tectonic Movements on Stresses and Deformations in Earth Embankments, Earthquake Engineering Research Center, University of California at Berkeley, Report No. UCB/EERC-90/13, 1990.

[7] Bray J.D., The Effect of Tectonic Movements on Stresses and Deformations in Earth Embankments. Ph.D. Dissertation., University. of California, Berkeley, 1990.

[8] Lazarte C.A.,The Response of Earth Structures to Surface Fault Rupture, Ph.D. Dissertation., University of California, Berkeley, 1996.

[9] Anastasopoulos I., Gazetas G.,Foundation–Structure Systems Over a Rupturing Normal Fault: Part I. Observations After the Kocaeli 1999 Earthquake, Bulletin of Earthquake Engineering, 2007, 5, 253–275.

[10] Mahdavian A., Rudbar Lorestan Dam Design and Local Faults. Proceedings of the 14th International Conference on Earthquake Engineering, 2008; Beijing, China.

[11] Bonilla M.G., Lienkaemper J.J., Visibility of Fault Strands in Exploratory Trenches and Timing of Rupture Events, Geology, 1990, 18, 153-156.

[12] Cole D.A. Jr., Lade PV, Influence Zones in Alluvium Over Dip-Slip Faults, Journal of Geotechnical Engineering Division, ASCE, 1984, 110 (5), 599-615.

[13] Johansson J., Konagai K., Fault Induced Permanent Ground Deformations- An Experimental Comparison of Wet and Dry Soil and Implications for Buried Structure, Soil Dynamics and Earthquake Engineering, 2006, 26, 45–53.

[14] Lin M.L., Chung C.F., Jeng F.S., Deformation of Overburden Soil Induced by Thrust Fault Slip, Engineering Geology, 2006, 88, 70–89.

[15] Moosavi S.M., Jafari M.K., Kamalian M., Shafiee A., Experimental Investigation of Reverse Fault Rupture–Rigid Shallow Foundation Interaction, International Journal of Civil Engineering, 2010, 8 (2), 85-98.

[16] Bray J.D., Seed R.B., Seed H.B., Analysis of Earthquake Fault Rupture Propagation Through Cohesive Soil, Journal of Geotechnical Engineering, 1994, 120,(3), 562-580.

[17] Johansson J., Konagai K., Fault Induced Permanent Ground Deformations: Experimental Verification of Wet and Dry Soil, Numerical Findings' Relation to Field Observations of Tunnel Damage and Implications for Design, Soil Dynamics and Earthquake Engineering, 2007, 27, 938–956.

[18] Bransby M.F, Davies M.C.R, El Nahas A., Centrifuge Modelling of Normal Fault–Foundation Interaction, Bulletin of Earthquake Engineering, 2008, 6, 585–605.

[19] Bransby M.F., Davies M.C.R., El Nahas A., Centrifuge Modelling of Reverse Fault–Foundation Interaction, Bulletin of Earthquake Engineering, 2008, 6, 607–628.

[20] Loukidis D., Bouckovalas G.D, Papadimitriou A.G., Analysis of Fault Rupture Propagation Through Uniform Soil Cover, Soil Dynamics and Earthquake Engineering, 2009, 29, 1389-1404.

[21] Swiger W.F., Specialty Session on Design for Fault Displacement, ASCE Specialty Conference, Earthquake Engineering and Soil Dynamics, 1978.

[22] Leps T.M., The Influence of Possible Fault Offsets on Dam Design, Water Power and Dam Construction, 1989, April, 36-43.

[23] Allen C.R., Cluff L.S.,Active Faults in Dam Foundations: An Update. Proceedings of 12th World Conference on Earthquake Engineering, 2000, Auckland, New Zealand.

[24] Cheney J.A., Shen C.K., Ghorayeb F., Fault Movement: Its Potential Damage to Embankment Dams, Proceedings of 8th World Conference on Earthquake Engineering, 1984, San Francisco, California, 341-347.

[25] Sohn J.S., Crack Propagation in Earth Embankments Subjected to Fault Movement, Ph.D. Dissertation., University. of California, Davis, 1987.

[26] Mejia L., Walker J., Gillon M., Seismic Evaluation of Dam on Active Surface Fault, Proceedings of Waterpower XIV Conference, 2005, Austin, Texas.

[27] Zania V., Tsompanakis Y., Psarropoulos P.N., Fault Rupture and Kinematics Distress of Earth Filled Embankments, Proceedings of the 14th International Conference on Earthquake Engineering, 2008, Beijing, China.

[28] Vafaie J., Taghikhany T., Tehranizadeh M., Near field effect on horizontal equal-hazard spectrum of Tabriz city in north-west of Iran, International Journal of Civil Engineering, 2011, 9 (1), 49-56.

[29]

Miraboutalebi M., Askari F., Farzaneh O., Effect of bedrock inclination on seismic slope stability according to Iran seismically data, International Journal of Civil Engineering, [30] 2011, 9 (4), 247-254.
Abaqus user's manual, version 6.10, Dassault Systèmes, 2012, [31] http://www. simulia. com
Menetrey P., Willam K., A Triaxial Failure Criterion for Concrete and Its Generalization, ACI Structures Journal, 1995, [32] 92, 311-318.
Roscoe K.H., The Influence of Strains in Soil Mechanics, Tenth [33] Rankine Lecture, Geotechnique 1970, 20 (2), 129-170.
James R.G., Bransby P.L., A Velocity Field for Some Passive Earth Pressure Problems, Geotechnique, 1971, 21 (1)1, [34] 61- 83.
Mortazavi Zanjani M., Soroush A., Solhmirzaei R., Near Surface Distortion Under Fault Rupture Propagation Through Soil, Proceedings of the 1st International Conference on Urban Construction in the Vicinity of Active Faults, 2011, Tabriz,